

Solidification of an alloy cooled from above. Part 3. Compositional stratification within the solid

By ROSS C. KERR,^{1†} ANDREW W. WOODS,^{1,2}
M. GRAE WORSTER,^{1‡} AND HERBERT E. HUPPERT^{1,2}

¹Department of Applied Mathematics and Theoretical Physics,

²Institute of Theoretical Geophysics, University of Cambridge,
Silver Street, Cambridge CB3 9EW, UK

(Received 22 June 1989)

This is the third of a series of papers which investigates the evolution of a binary alloy that is cooled from above and releases buoyant residual fluid as one component of the alloy is preferentially incorporated within the solid. This paper focuses on the compositional zonation that is produced when the melt is completely solidified. Parts 1 and 2 considered the temperature of the cooled boundary to be greater than the eutectic temperature of the alloy so that only partial solidification of the alloy could occur. Here we extend the study by investigating the effects that arise when the cooling temperature is less than the eutectic temperature. The formation of a completely solid layer results, which extends from the cooling plate down to a mushy zone of dendritic crystals and interstitial melt. The melt below this mushy layer is convectively unstable because it is cooled from above. This generates vigorous thermal convection. Eventually the melt becomes completely solidified and a compositionally zoned solid is formed. The solid below the cooling plate is shown to be of fixed bulk composition until it reaches the depth that the interface between the mushy layer and melt occupied when the melt first became saturated. Below this level, the composition of the solid decreases with depth until it merges into the solid growing from the floor, whose composition is nearly equal to that of the heavier component of the alloy. Results of laboratory experiments with aqueous solutions of sodium sulphate are in good agreement with our quantitative predictions. The model is used to give an interpretation of profiles of the composition of magnesium oxide found within solidified komatiite lavas.

1. Introduction

The influence of convection in the melt during the solidification of alloys is very important in generating compositional zonation within solids. This has significant geological implications for the interpretation of solidified bodies of magma. It is also of great importance in metallurgy and material science in the production of cast alloys. This paper continues investigations (Kerr & Turner 1982; Huppert *et al.* 1987; Woods & Huppert 1989) of the mechanisms of generating solids that are compositionally stratified. We analyse the complete solidification of a binary melt

† Present address: Research School of Earth Sciences, Australian National University, GPO Box 4, Canberra, Australia.

‡ Present address: Department of Engineering Sciences and Applied Mathematics and Department of Chemical Engineering, Northwestern University, Evanston, IL 60208, USA.

whose composition exceeds the eutectic composition and which is cooled from above at a temperature less than its eutectic temperature. The eutectic point defines the composition of the melt at the minimum temperature at which, under thermodynamic equilibrium, it is in the liquid state. For the alloys considered here, the density of the melt is assumed to increase with composition (at fixed temperature) and the heavy component of the melt is preferentially incorporated into the solid to release a light residual. We extend and develop the model introduced in Part 2 (Kerr *et al.* 1990*b*) in order to investigate the production of the solid eutectic layer. This solid layer forms above a partially solidified zone, called a mushy layer, in the region where the local temperature is less than the eutectic temperature. We determine the nature of the stratification and examine the processes generating such zoned solid.

Kerr & Turner (1982) investigated experimentally the solidification of multi-component aqueous solutions cooled from below. They produced multi-layered solids by a mechanism of selective solidification of different components. The solidification of a binary alloy cooled from vertical and sloping sidewalls was investigated by Huppert *et al.* (1987). In a series of solidification experiments they produced complex crystal morphologies in solids which were zoned in both the vertical and horizontal directions. Woods & Huppert (1989) concentrated upon the solid grown by cooling a binary alloy from below, in contrast to the present study of cooling from above. They presented a theory for the convection of the melt driven by the release of compositionally buoyant residual fluid. The predictions of the compositional layering in the solid produced by this convection were successfully compared with some experimental investigations using aqueous sodium carbonate.

Chen & Turner (1980) and Turner, Huppert & Sparks (1986, herein referred to as THS) carried out experiments in which aqueous solutions whose compositions were greater than the eutectic composition were cooled and solidified from above. In their investigatory experiments, Chen & Turner (1980) observed a number of the qualitative features that we describe and quantify, including the growth of solid on both the roof and floor of the tank and the development of vigorous thermal convection in the melt. THS conducted a number of experiments using several different aqueous solutions in which they measured the compositional zonation of the solid. They also introduced and analysed a model for the growth of solid of eutectic composition. The more detailed model that we have developed for a general two-component melt, which incorporates governing equations for a mushy region and allows for effects of disequilibrium, enables predictions to be made of the compositional zonation of the solid.

In Parts 1 and 2 (Kerr *et al.* 1990*a, b*) we investigated the partial solidification of an alloy that occurs when the cooling plate is maintained at a temperature greater than the eutectic temperature. In Part 1, we described an equilibrium model for the growth of a mushy layer using local conservation laws for the transfer of mass and heat. In Part 2 we introduced a simple non-equilibrium growth law, which relates the rate of advance of the interface between the melt and the mushy layer to the difference, δT , between the saturation temperature of the melt and the temperature at the base of the interstitial melt, given by

$$\frac{dh_i}{dt} = \mathcal{G}\delta T, \quad (1.1)$$

where \mathcal{G} (which is a positive constant) is determined empirically. This growth law reflects the fact that, in order for crystals to grow, the melt must cool below its

saturation temperature. This allows crystals of the heavy component to form in the melt, lowering the composition of the melt and also heating the melt through the release of latent heat. These crystals settle out of the melt and gather on the base of the tank. As the composition of the melt falls, the bulk composition of the mushy layer that subsequently forms above the melt also falls. Consequently, when the roof temperature is maintained at a temperature less than the eutectic, the solid that forms above the mushy layer is compositionally zoned. We investigate this situation in the present paper.

In §2, we describe some laboratory experiments in which aqueous solutions of sodium sulphate were completely solidified by cooling from above. In §3 we consider the general features of the solidification process, introduce the detailed mathematical model and discuss the kinetic growth law (1.1) in further detail. In §4 we describe the numerical solution of the governing equations of the model and compare the theoretical predictions with the experimental results. In §5 we compare the predictions of our model with some field data of solidified komatiite lavas that were cooled from above, as described in THS. The major conclusions of the study are presented in §6.

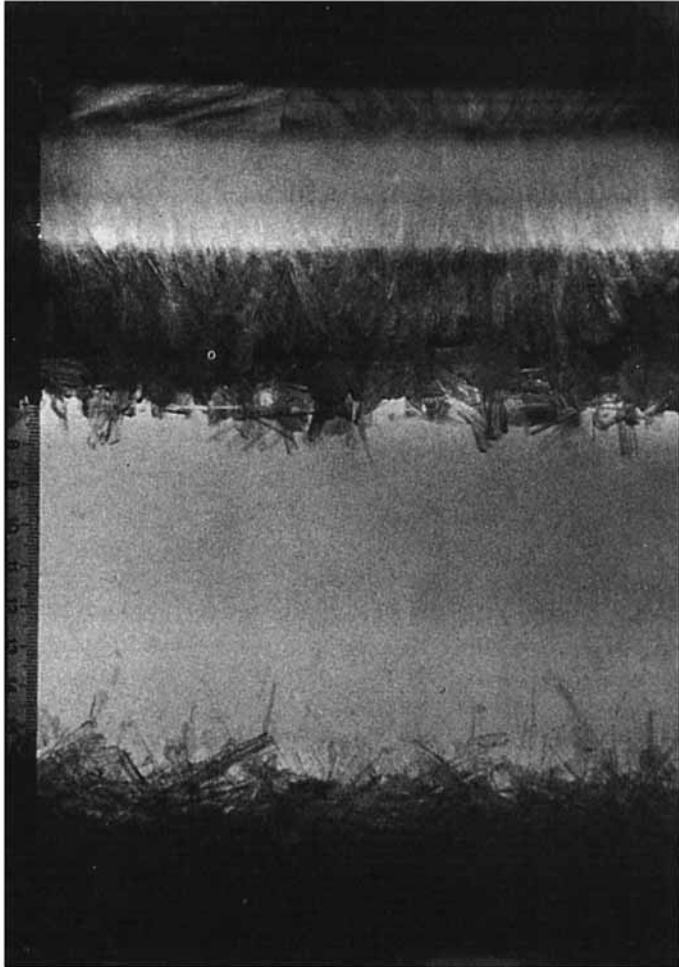
2. Laboratory experiments

Experiments were conducted in which aqueous solutions of sodium sulphate (Na_2SO_4) of composition beyond the eutectic composition were completely solidified by cooling from above, with the cooling plate maintained well below the eutectic temperature. Aqueous Na_2SO_4 was chosen because its eutectic temperature is relatively high (-1.2°C) compared with the temperature which the cooler could achieve (-30°C). As a consequence, complete solidification of the melt could occur before unwanted heat transfer from the environment became significant. The experiments were conducted in a $20 \times 20 \times 18.8$ cm high tank with an upper brass plate through which coolant could be pumped from a cooling unit, as described in Part 1.

In each experiment the temperature of the plate was maintained at a fixed value after an initial transient which lasted approximately 30 min. Convective motion in the tank was observed using the shadowgraph technique. In addition, the variations with time of the depths of the roof solid layer, the mushy layer and the basal solid layer were measured. After the melt had solidified completely, the solid block was removed from the tank and cut with a hack-saw into blocks of about 1 cm thickness, to determine the vertical distribution of composition; this was done by diluting the sample with water and measuring its refractive index with a hand-held refractometer. The refractive index was then related to the composition using data from Weast (1971). During the measurement of the composition, in particular when the sections were being cut, some selective melting of the ice within the solid occurred; this possibly led to an increase of up to 10% in the measured composition.

On starting each experiment a composite solid layer rapidly formed below the roof. After a short time (≈ 5 min) a mushy layer between the solid and melt could be discerned. The interstitial melt between the dendrites subsequently solidified from above to form composite solid. A few hours after the start of each experiment, a thin layer of crystals settled and began to grow on the base of the tank. The photograph in figure 1(a) shows the nature of the mush, melt and solid during a typical experiment with aqueous Na_2SO_4 and a schematic diagram of this configuration is shown in figure 1(b).

(a)



(b)

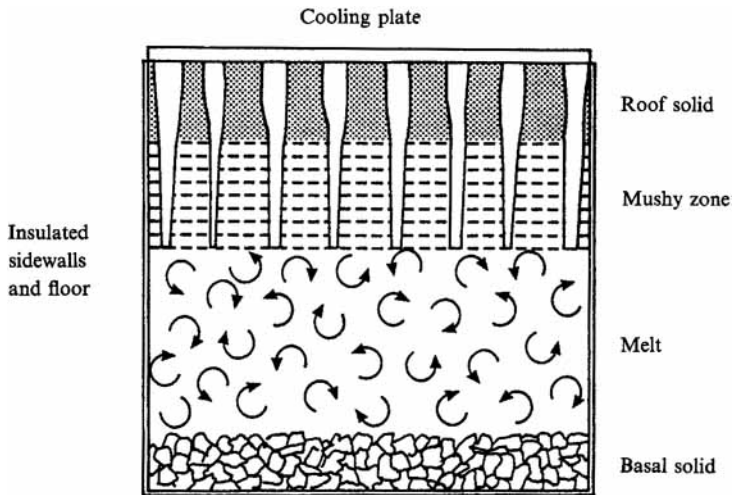


FIGURE 1 (a, b). For caption see facing page.

(c)

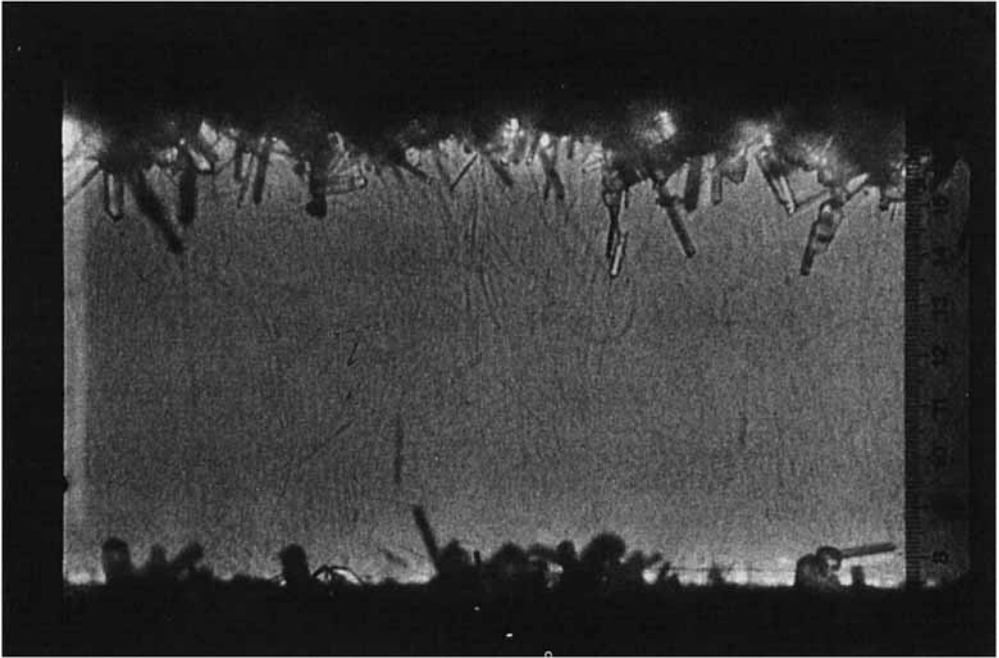


FIGURE 1. (a) Photograph showing the basal solid, the melt, the mushy layer and the roof solid in a typical experiment in which aqueous Na_2SO_4 was solidified from above. (b) A schematic diagram of the configuration of the solid, mush and melt, showing in a qualitative way the morphology of the solid. (c) Photograph of a typical experiment in which aqueous Na_2SO_4 was solidified from above, which shows the convection in the melt and the density jump at the interface between the mushy layer and the melt.

A few minutes after the start of the experiment, strong thermal convection developed in the melt and this appeared to mix the melt very efficiently. The growth of basal solid released plumes of compositionally depleted fluid from the floor. These rose into the convecting melt and enhanced the thermal convection. However, shadowgraph observations indicate that near the interface between the mushy layer and the melt, the downflowing thermal plumes dominated the motion until a late stage in the experiment, when nearly all the melt had solidified. The thinner, compositionally buoyant plumes appeared to mix into the ambient fluid, possibly by means of shear instabilities, before reaching this interface. A typical photograph of the convection is shown in the photograph in figure 1(c). After about 30 h, the convection in the melt became very sluggish, the mushy layer became very thin and the plumes of compositionally depleted fluid being released from the basal solid disappeared; this suggests that the composition of the melt had become very close to the eutectic composition.

The photograph in figure 2, taken at the end of an experiment with aqueous Na_2SO_4 , shows the typical morphology of the final solid produced by the experiments. The crystal structure of the solid varies with depth. Near the top of the solid, in the region through which the dendritic mushy layer passed, long, regular, vertically aligned crystals can be seen. Further down the solid, a band of more homogeneous, eutectic solid has formed. This corresponds to the stage when the melt had ceased to convect vigorously and its composition had become close to eutectic. The lower third

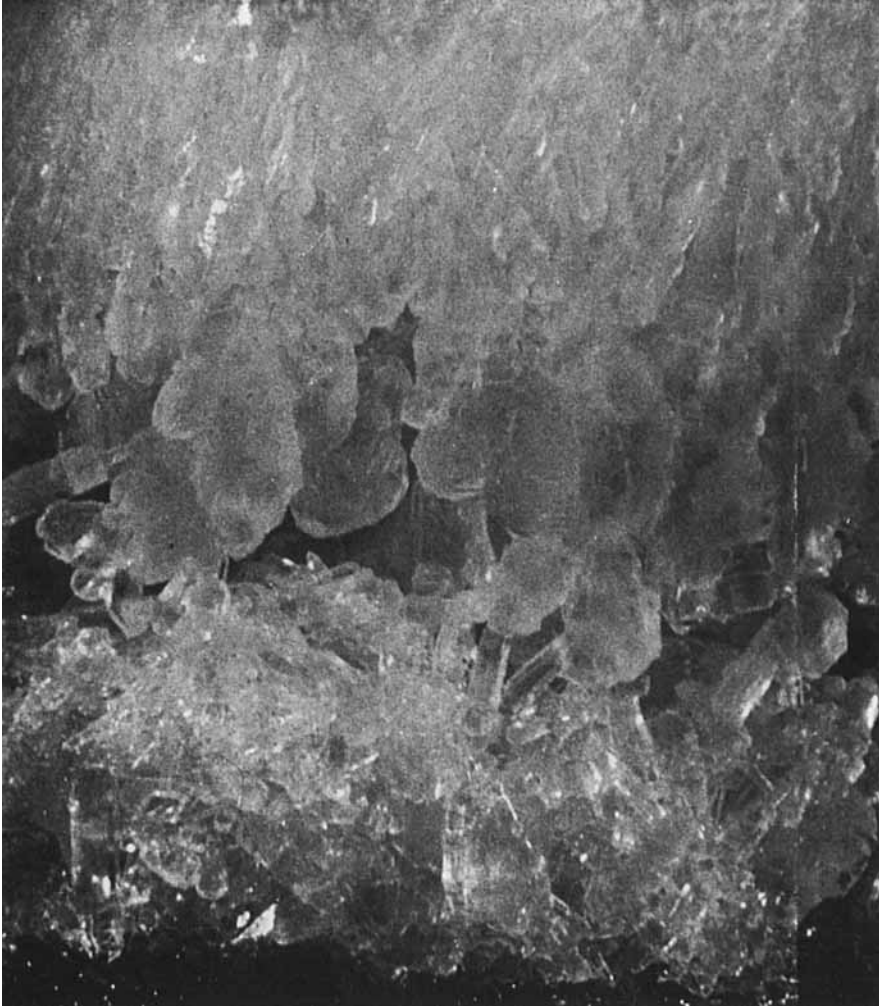


FIGURE 2. Photograph of final solid product formed from an initially homogeneous aqueous solution of Na_2SO_4 , showing the morphology and zonation of the crystals of $\text{Na}_2\text{SO}_4 \cdot 10\text{H}_2\text{O}$ within the solid.

of the solid consisted of irregular, randomly oriented basal solid crystals that had grown at the floor.

The dendritic crystals in the mushy layer became faceted a few hours after the start of each experiment. The very fine, 'pine-tree' structure of the dendritic crystals evolved into angular crystals with planar surfaces. At the same time, the process of Ostwald ripening (Glicksman & Voorhees 1984; Doremus 1985), whereby small crystals disappear and larger crystals grow in order to minimize surface energy, became important. This effect increases the size of the dendrites and the interdendrite spacing (cf. Part 2) and may reduce the accuracy of using a continuum approximation to model the mushy layer, although we note that it did not appear to affect the results presented in Part 2. However, more importantly, the large crystals can create difficulties in obtaining a representative sample of the solid to measure its composition, because the mushy layer may cease to be laterally homogeneous on a

scale convenient for sampling the solid block. In order to minimize such errors we carried out an experiment in which we sampled all the solid.

In §4, we discuss the quantitative results of these experiments and compare these with the predictions of our theory.

3. A model for the complete solidification of a melt

We now extend the mathematical model introduced in Parts 1 and 2, which describes the evolution of the temperature and composition in the melt, mushy and basal solid layers, to include the formation of solid at the roof, above the mushy layer. The solidification history has two distinct temporal phases; initially a composite solid grows directly from the melt, but after a short period of time an intermediate mushy zone forms, as described in §2. The majority of the growth occurs after the mushy layer has formed, and we develop a general model for this stage of the solidification. We then adapt the model for application to the solidification during the initial phase and consider the conditions at the onset of the development of the mushy layer.

We assume that the solidification is subject to the same principles of thermodynamics as described in Parts 1 and 2. The temperature of the cooling plate is maintained below the eutectic temperature so that a layer of solid forms below the plate. This solid layer, which grows above the mushy zone, consists of dendrites connected by solidified interstitial melt, as shown schematically in figure 1(b). We refer to this region as the *roof solid*. The bulk composition of this solid, C_H , may be defined in terms of the horizontal average of its constituents. If the horizontal average of the volume fraction of dendritic crystals is ϕ , the composition of the solidified interstitial melt is C_s and the dendritic crystals have composition C_β then the bulk solid composition is given by

$$C_H = \phi C_\beta + (1 - \phi) C_s. \quad (3.1)$$

The composition, C_s , and latent heat of fusion per unit volume, \mathcal{L}_s , of the solidified interstitial melt may be determined in terms of the volume fraction, $\hat{\phi}$, of pure component β in this solid by

$$C_s = \hat{\phi} C_\beta + (1 - \hat{\phi}) C_\alpha \quad (3.2)$$

and

$$\mathcal{L}_s = \hat{\phi} \mathcal{L}_\beta + (1 - \hat{\phi}) \mathcal{L}_\alpha, \quad (3.3)$$

where the subscript α is used to denote properties of the pure solid of the light component in the melt, β the properties of the pure solid of the heavy component in the melt and s the composite solid formed from the interstitial melt. We deduce that, in order to produce roof solid that is stratified, either the solid fraction at the interface between the solid and the mushy layer or the composition of the solidified interstitial melt must evolve with time.

Since the temperature of the melt never fell below the eutectic temperature in our experiments, the solid that forms at the base of the chamber, by crystallization from the saturated melt, has composition C_β . We refer to this region as the *basal solid*. As the basal solid forms and releases fluid depleted of component β , the composition of the melt falls. Therefore the melt subsequently incorporated into the mushy layer is compositionally depleted and in turn the bulk composition of the mushy layer and thus of the roof solid decreases.

The geometry of the mathematical model is depicted in figure 3. The roof solid

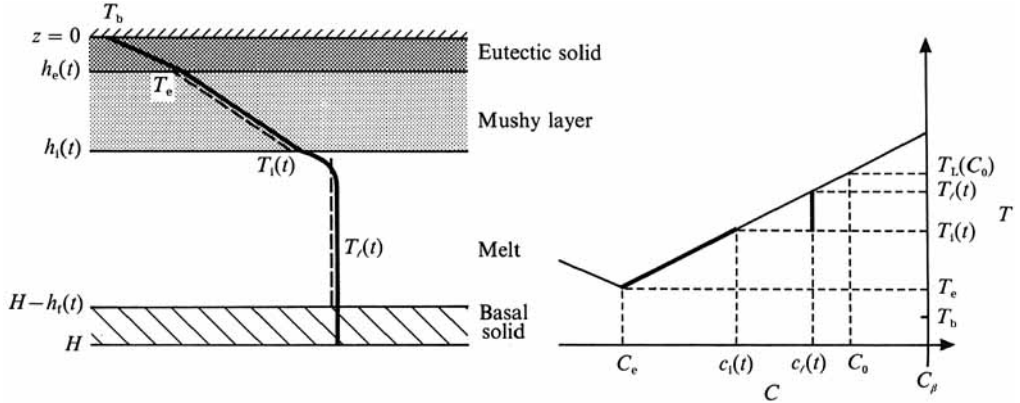


FIGURE 3. The profiles of the composition and temperature in the various regions which develop during the solidification. The interstitial melt lies on the liquidus and the dendritic crystals have the composition of pure component β . The jump in the temperature and composition at the interface between the mushy layer and the melt is produced by the disequilibrium necessary for the mush growth.

occupies the region $0 \leq z \leq h_e$, the mushy layer $h_e \leq z \leq h_1$, the melt $h_1 \leq z \leq H - h_1$ and the basal solid $H - h_1 \leq z \leq H$. The roof temperature is T_b , which is fixed. The temperature at the interface between the mushy layer and the solid is T_e , the eutectic temperature, and the temperature between the mushy layer and the melt is $T_i(t)$, which varies with time. For simplicity, we assume that the melt and basal solid have the same uniform temperature, T_ℓ , which also varies with time. This approximation will be reasonable if the convection in the melt is sufficiently vigorous and the thermal conduction across the solid sufficiently rapid. The composition of the interstitial melt is $C(z)$ and the composition of the melt is C_ℓ . The initial temperature and composition of the melt are T_0 and C_0 . The very fine horizontal structure of the mushy layer allows lateral diffusion to remove any horizontal gradients in the interstitial melt; therefore we approximate the process as one-dimensional.

Before introducing the governing equations for the solidification process, we define horizontal averages of the physical properties of the solid and mushy layer which are needed for the modelling. This is necessary because for many materials the solid and melt may have very different physical properties. We assume that the parallel law for the conductivities of composite materials holds for the present system as discussed in Batchelor (1974) and Part 1. In the eutectic solid region the bulk specific heat per unit volume and the bulk thermal conductivity are then given by

$$c_H = \left(\frac{C_H - C_\alpha}{C_\beta - C_\alpha} \right) c_\beta + \left(1 - \frac{C_H - C_\alpha}{C_\beta - C_\alpha} \right) c_\alpha \tag{3.4}$$

and
$$k_H = \left(\frac{C_H - C_\alpha}{C_\beta - C_\alpha} \right) k_\beta + \left(1 - \frac{C_H - C_\alpha}{C_\beta - C_\alpha} \right) k_\alpha. \tag{3.5}$$

Note that in this paper we set $C_\alpha = 0$.

The averaged properties in the mushy layer are given by

$$c_m = \phi c_\beta + (1 - \phi) c_\ell \tag{3.6}$$

and
$$k_m = \phi k_\beta + (1 - \phi) k_\ell, \tag{3.7}$$

where the subscript ℓ denotes properties of the melt, which are assumed to be constant, and m denotes properties of the mushy layer.

We now introduce the heat and mass conservation equations which apply in the different regions and consider the interfacial boundary conditions. Initially the temperature of the melt is greater than the liquidus temperature and so no basal solid forms. However, once the temperature of the melt falls to the liquidus temperature, internal solidification of the melt can occur. We assume that the internal crystal growth forms a solid layer at the base of the fluid region and that it occurs sufficiently rapidly that the melt is kept in thermodynamic equilibrium. In the analysis presented below we formally include terms representing the effects of the basal solid throughout; however, these are only non-zero after the melt becomes saturated.

We start by considering the roof solid which satisfies the thermal conduction equation

$$c_H \frac{\partial T}{\partial t} = \frac{\partial}{\partial z} \left(k_H \frac{\partial T}{\partial z} \right). \quad (3.8)$$

We note that the compositional diffusivity of the solid is so small that there is negligible transport of the solute in the solid during the timescale of interest. At the interface between the solid and the mushy layer, conservation of energy requires

$$k_H \frac{\partial T}{\partial z} \Big|_{h_e^-} = k_m \frac{\partial T}{\partial z} \Big|_{h_e^+} + \mathcal{L}_s (1 - \phi) \frac{dh_e}{dt}. \quad (3.9)$$

Neglecting the diffusion of composition in the solid, we obtain the corresponding relation for the conservation of composition at the interface between the solid and the mushy layer

$$\frac{dh_e}{dt} (C_s - C_e) = D \frac{\partial C}{\partial z} \Big|_{h_e^+}, \quad (3.10)$$

where D is the compositional diffusivity of the melt. Comparison of (3.9) and (3.10) suggests that the flux of composition from the interstitial melt at the boundary between the mushy layer and the solid is very small, since the ratio $D/\kappa \ll 1$, where κ is the thermal diffusivity of the melt. We deduce from (3.10) that

$$C_s = C_e. \quad (3.11)$$

In thermodynamic equilibrium, the interstitial melt lies on the liquidus

$$T = T_L(C). \quad (3.12)$$

In general this is a nonlinear curve which we approximate using a cubic spline. The equations governing the diffusion of heat and solute in the mushy layer (Worster 1986) are, on adopting the notation of Part 1,

$$\frac{\partial}{\partial z} \left(k_m \frac{\partial T}{\partial z} \right) = c_m \frac{\partial T}{\partial t} - \mathcal{L}_\beta \frac{\partial \phi}{\partial t} \quad (3.13)$$

and

$$\frac{\partial}{\partial z} \left(D(1 - \phi) \frac{\partial C}{\partial z} \right) = \frac{\partial}{\partial t} ((C - C_\beta)(1 - \phi)). \quad (3.14)$$

Again since $D/\kappa \ll 1$ we deduce from (3.12)–(3.14) that the vertical transport of composition in the mushy layer is negligible.

At the interface between the mushy layer and the melt, the conservation of heat requires

$$k_m \frac{\partial T}{\partial z} \Big|_{z=h_1^-} = \mathcal{L}_\beta \phi h_1 + F_T + \frac{dh_1}{dt} (T_\ell - T_1) c_\ell. \quad (3.15)$$

This relationship balances the thermal flux conducted away through the mushy layer with three source terms. First, the rate of production of latent heat as the dendritic crystals advance into the melt; second, the convective heat flux from the melt, F_T ; and third, the thermal energy released when the melt is cooled as it is incorporated into the mushy layer. We evaluate F_T by using the empirical law, introduced in Part 1, for the convective heat transfer from a high-Rayleigh-number, thermally convecting melt,

$$F_T = Nu \left(\frac{k_\ell \Delta T}{H} \right) \left(\frac{T_\ell - T_i}{\Delta T} \right)^{\frac{3}{2}}, \quad (3.16)$$

where $\Delta T = T_L(C_0) - T_e$, the Nusselt number $Nu = 2^{\frac{3}{2}} \lambda (\alpha g \Delta T H^3 / \nu \kappa_\ell)^{\frac{1}{2}}$, α is the coefficient of thermal expansion of the melt and ν the kinematic viscosity. As discussed in Part 1, $\lambda \approx 0.056$ for the heat flux into a solid surface from a melt (Denton & Wood 1979). We use this value in the heat flux law at the interface between the mushy layer and the melt.

The conservation of composition across this interface takes the form

$$D \frac{\partial C}{\partial z} \Big|_{z=h_1^-} = - \frac{dh_1}{dt} (\phi C_\beta + (1-\phi) C|_{z=h_1^-} - C_\ell) + F_C. \quad (3.17)$$

This equation equates the flux of composition across the mushy layer with the rate of release of composition on incorporation of the melt into the mushy layer together with the compositional flux from the melt, F_C . We further assume that there is no convective flux of composition from the melt, $F_C \approx 0$, and so we obtain

$$\phi C_\beta + (1-\phi) C|_{z=h_1^-} = C_\ell. \quad (3.18)$$

Therefore the bulk composition at depth z in either the mushy layer or the final solid product equals that which the melt had at the previous time when the interface between the mushy layer and the melt was at position z . This means that

$$\phi(z, t) = \frac{C_\ell(t^*) - C(z, t)}{C_\beta - C(z, t)}, \quad (3.19)$$

where t^* is the time at which $h_1(t^*) = z$ and $C(z, t) = C_\ell(t^*)$. This may be recognized as the Scheil equation (Kurz & Fisher 1986) and is equivalent to (4.8) of Part 2. Therefore, the bulk composition of the roof solid, C_H , at position z equals the composition of the melt at the previous time, t^* , at which $h_1(t^*) = z$. By conservation of energy, the temperature of the melt evolves according to

$$[c_\ell(H - h_1) - (c_\ell - c_\beta)h_\tau] \frac{dT_\ell}{dt} = \mathcal{L} \frac{dh_\tau}{dt} - F_T. \quad (3.20)$$

Equation (3.20) balances the rate of change of internal energy of the melt and basal solid with the rate of production of latent heat on forming the basal solid together with the convective heat flux from the melt.

Using the approximation $F_C = 0$, the compositional evolution of the melt may be written

$$(H - h_1 - h_\tau) \frac{dC_\ell}{dt} = - \frac{dh_\tau}{dt} (C_\beta - C_\ell). \quad (3.21)$$

Again we note that when the melt is unsaturated, $h_\tau = 0$.

In the basal solid, which forms when the melt is cooled and saturated, the temperature is assumed to be the same as in the melt,

$$T = T_\ell \quad \text{and} \quad C = C_\beta. \quad (3.22 a, b)$$

In Part 2 we introduced a simple growth law, based on the hypothesis that the growth of the dendritic mushy layer depends on the supersaturation at the interface between the mushy layer and the melt. We assumed that the growth rate, dh_i/dt , depends linearly on this supersaturation, giving

$$\frac{dh_i}{dt} = \mathcal{G}(T_L(C_\ell) - T_i), \quad (3.23)$$

where the parameter \mathcal{G} is determined empirically. In Part 2, the predictions of this kinetic growth law were shown to agree well with experiments in which a mushy layer was grown from aqueous solutions of both sodium sulphate and isopropanol cooled at a temperature greater than the eutectic temperature.

When the cooling plate is maintained at a temperature less than the eutectic temperature, the experimental observations (§2) indicate that there is an initial stage of solidification in which a layer of composite solid with an approximately flat interface forms on the cooling plate. Only after approximately five minutes does a discernible mushy layer develop below the solid. We now model the solidification before the mushy layer develops and introduce a condition for the onset of its growth.

We apply the kinetic growth law (3.23) for the initial growth of the solid by allowing the temperature at the interface between the solid and melt, which we denote by T_i , to fall below the eutectic temperature, T_e . The kinetic growth law for modelling the growth of such eutectic solid becomes (cf. (3.23))

$$\frac{dh_e}{dt} = \mathcal{G}(T_L(C_\ell) - T_i). \quad (3.24)$$

In addition, the growth of this solid layer is constrained by the conservation of thermal energy across the interface (cf. (3.9), (3.15))

$$(\mathcal{L}_c + c_\ell(T_\ell - T_i)) \frac{dh_e}{dt} + F_T = -k_s \left. \frac{\partial T}{\partial z} \right|_{h_e^-}. \quad (3.25)$$

The temperature of the roof is T_b and so initially

$$T_i = T_b, \quad h_e = 0, \quad T_\ell = T_0 \quad \text{and} \quad C_\ell = C_0. \quad (3.26)$$

We postulate that the mushy layer begins to develop when $T_i = T_e$, and use the conditions in the system at this point as the initial conditions for the subsequent growth of the system including a mushy layer, described earlier. In practice, this initial regime does not last very long before the mushy layer forms (at most a few minutes in an experiment lasting forty hours) and so any errors introduced by this pre-mush solidification model will not be significant at a later stage in the experiment.

4. Solution of the model equations for total solidification

The governing equations presented in the previous section were solved using a second-order, implicit, predictor-corrector scheme in conjunction with the Thomas

Parameter	Value	Units
α	$(5.0 + 0.24(T - 20)) \times 10^{-4}$	$^{\circ}\text{C}^{-1}$
ν	0.015	$\text{cm}^2 \text{s}^{-1}$
c_f	4.14	$\text{J cm}^{-3} ^{\circ}\text{C}^{-1}$
c_β	2.66	$\text{J cm}^{-3} ^{\circ}\text{C}^{-1}$
c_α	1.75	$\text{J cm}^{-3} ^{\circ}\text{C}^{-1}$
k_f	0.0059	$\text{W cm}^{-1} ^{\circ}\text{C}^{-1}$
k_β	0.0080	$\text{W cm}^{-1} ^{\circ}\text{C}^{-1}$
k_α	0.022	$\text{W cm}^{-1} ^{\circ}\text{C}^{-1}$
\mathcal{L}_α	307	J cm^{-3}
\mathcal{L}_β	337	J cm^{-3}
$T_i(C_0)$	20.0	$^{\circ}\text{C}$
T_b	-17.0	$^{\circ}\text{C}$
T_e	-1.2	$^{\circ}\text{C}$
T_0	30.1	$^{\circ}\text{C}$
λ	0.056	—

TABLE 1. The parameter values used to calculate the evolution of the experiments

Algorithm, as described by Ames (1977). Initially, only one computational domain was required, spanning the composite solid region. The growth of the mushy layer was assumed to commence when T_i reached T_e , at which time a second computational domain was introduced spanning the mushy region.

Calculations were made using the experimental parameters given in table 1 and $\mathcal{G} = 1.5 \times 10^{-4} \text{ cm s}^{-1} \text{ K}^{-1}$, the value of the kinetic growth parameter which was found in Part 2 for aqueous Na_2SO_4 . Typical results are shown in figure 4 which depicts the evolution of the thickness of the mushy layer, roof and basal solid layers (figure 4*a*) and the melt and interface temperatures (figure 4*b*). The mushy layer is predicted to grow very soon after the start of the experiment and it then advances ahead of the solid layer. The melt cools down rapidly and after approximately 30 min becomes saturated. At this point the basal solid begins to grow, somewhat less rapidly than the roof solid. The mushy layer and basal solid meet after approximately 35 h, by which stage the composite roof solid occupies approximately two-thirds of the depth of the tank. It may be seen that the variation with time of the temperature at the interface between the mushy layer and the melt exhibits somewhat similar changing physical balances as described in Parts 1 and 2.

The variation of the solid composition with depth is shown in figure 5. Just below the roof, the solid has a fixed composition equal to the initial composition of the melt. The composition only begins to decrease below the depth that the mushy layer had when the melt first became saturated. It then falls steadily with depth until the depth at which the mushy layer and the basal solid converge. Below this point, the solid is of composition C_β .

Measurements made during one of the experiments described in §2 have been included in figures 4 and 5 for comparison with the model. This experiment corresponds to the data given in table 1. There is very good agreement between the predictions of the model and the experimental measurements of the thickness of the roof solid, mushy layer and basal solid as functions of time (figure 4*a*) and also the melt temperature (figure 4*b*). However, one difference is that after approximately 100 min the melt is observed to become a little supersaturated (about 1°C) in comparison with the theoretical predictions. The supersaturation in the melt arises in part owing to the experimental problem of nucleation in the initiation of crystal

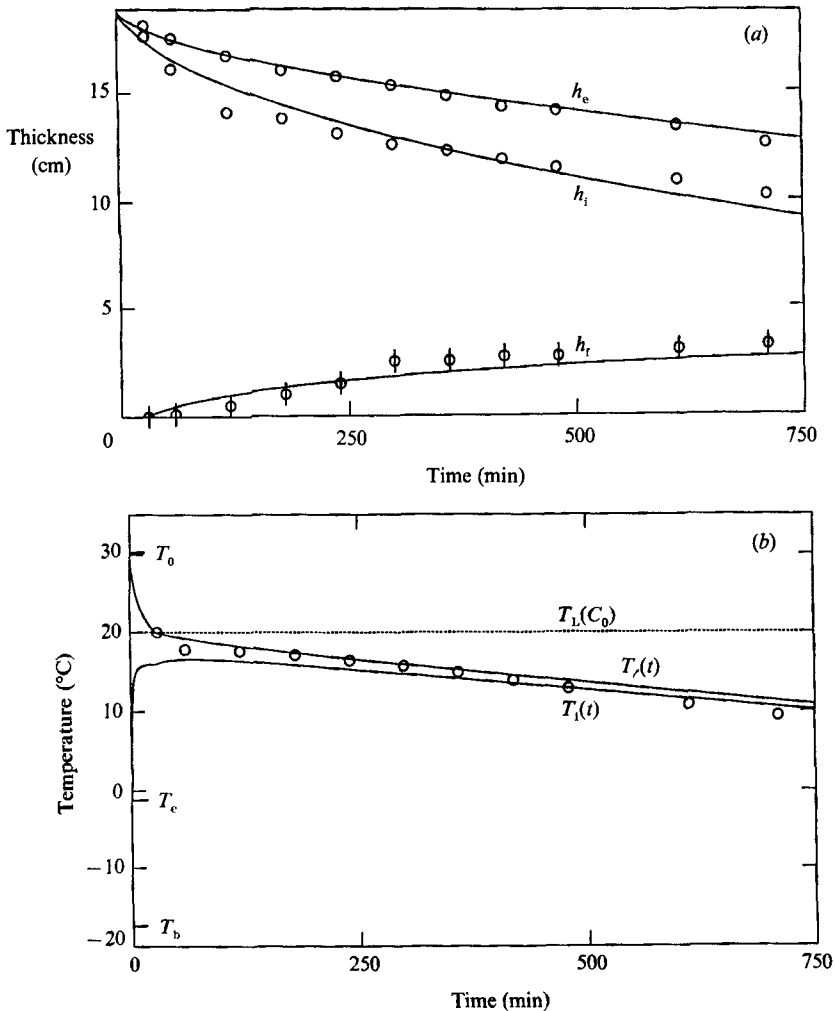


FIGURE 4. (a) Predicted and experimentally measured growth of the mushy (h_i), roof (h_e) and basal solid (h_r) layers as functions of time; (b) predicted evolution of the melt T_r and interface T_i temperature with time. The experimental data are shown as circles. In the calculations $\mathcal{G} = 1.5 \times 10^{-4} \text{ cm s}^{-1} \text{ }^{\circ}\text{C}^{-1}$ and the remaining parameters used to generate these curves are given in table 1.

growth, which restricts the growth of the basal solid. In contrast the model assumes that the basal solid grows sufficiently fast to restore the melt to thermodynamic equilibrium. This effect causes some discrepancy between the predicted and observed thicknesses of the mushy layer after about 150 min of the experiment; this is because in practice some crystals grow ahead of the position of the interface between the mushy layer and the melt that is predicted by the model and into the region of supersaturated melt ahead. A further consequence is that the composition of the roof solid measured in the experiments is greater than the prediction of the model, since the effective thickness of the mushy layer in the experiments is larger than the value predicted by the model during the early stages of the experiment.

The irregular structure of the basal solid and its non-planar interface with the overlying melt contrasts with the simple model of a flat uniform layer of basal solid described in §3; this can introduce an error of up to 0.5 cm in the measurements of

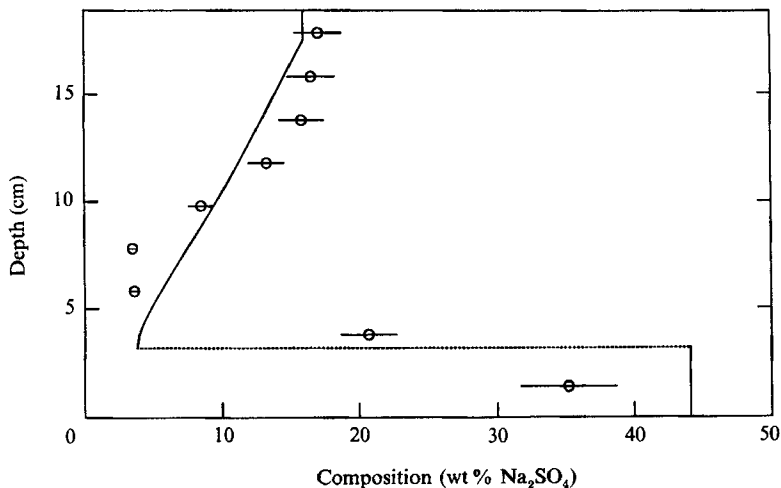


FIGURE 5. The variation of solid composition with depth calculated for the parameter values given in table 1 with $\mathcal{G} = 1.5 \times 10^{-4} \text{ cm s}^{-1} \text{ } ^\circ\text{C}^{-1}$. Experimental measurements are denoted by circles. It should be noted that errors of at most 10% arise owing to the melting of the sample during cutting.

the mean thickness of the basal solid, as indicated in figure 4(a). In addition, errors arise when measuring the composition of the solidified block as explained in §2. This may cause an overestimate of the composition of up to 10% as indicated on figure 5. However, despite these errors, the results provide strong evidence to support the model of the growth that we have developed.

As \mathcal{G} is increased the relative amount of basal solid to roof solid decreases. This is because as \mathcal{G} increases, the degree of supersaturation required for a given growth rate decreases (3.23). Therefore the interface temperature, T_i , is larger and so the heat flux from the melt, F_T , is smaller resulting in a slower evolution of the melt and basal solid. In figure 6, we show the variation of the structure of the compositional zonation as \mathcal{G} changes for the parameter values given in table 1. It can be seen that the solid becomes more strongly zoned as \mathcal{G} decreases, corresponding to the greater quantity of basal solid that forms.

We have investigated the effect of approximating the nonlinear temperature profile through the solid layer with a linear profile. The results of this approximate model are very similar to those of the full diffusion equation (3.8) when modelling the particular laboratory experiment described above. However, some small differences arise; in particular, the basal solid is predicted to grow faster in the simplified model (by at most 10%) and so the melt composition and thus temperature are predicted to evolve more rapidly. This results in the prediction of the composition of the roof solid being smaller than in the full model and also the temperatures of the melt predicted by this approximate model are 1–2 °C lower than in the full model. Note that the approximation of a linear temperature profile in the solid only ignores the contribution to the heat budget from the specific heat of the solid which is not very large at high Stefan number.

In order to improve the accuracy of the predictions of the model a more detailed study of the mechanism of the secondary solidification could be developed. This might include some of the features introduced both by Flood & Hunt (1987), in which the secondary solidification manifests itself as secondary crystals in the melt, and by the present model in which all the secondary solidification is assumed to occur on the floor of the chamber.

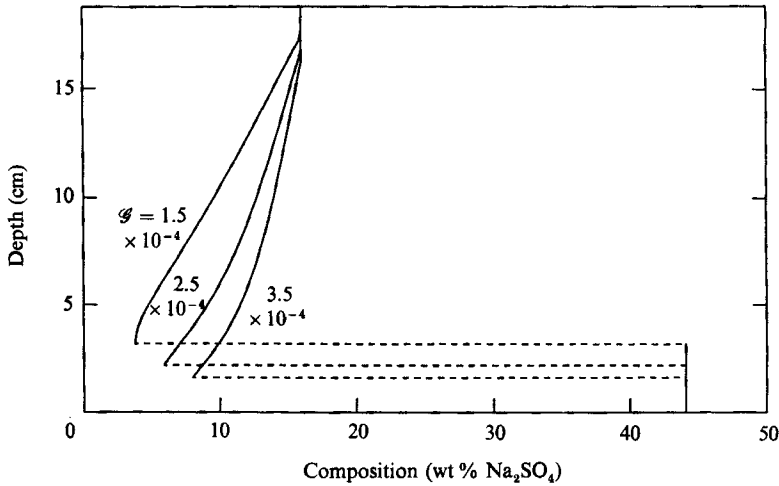


FIGURE 6. The compositional zonation in the solid for $G = 1.5, 2.5, 3.5 \times 10^{-4} \text{ cm s}^{-1} \text{ } ^\circ\text{C}^{-1}$. The calculations were made using the parameter values shown in table 1.

5. Geological implications

As suggested in Part 2, the solidification process outlined in this work is of significant interest for geologists in the interpretation of solidified deposits. In particular, in the submarine solidification of komatiite lavas, the main cooling is from above and this is analogous to the simple configuration that we have considered herein. The crystal morphologies and compositional zonation observed in komatiite deposits are similar to those produced in the solidification experiments described in §2. For example, figure 7 shows some measurements of the variation of MgO concentration with depth in several komatiite outcrops in Northern Ontario, Canada, as presented by THS. These may be compared with figure 6 herein. Various mechanisms for the formation of such zonation in solidifying magma have been suggested (Donaldson 1982; THS; Arndt 1986). These include (i) crystal settling from the convecting melt (Martin & Nokes 1988, 1989), (ii) increasing the concentration of crystals in suspension in the convecting layer until the melt can no longer convect (Huppert & Sparks 1986, 1988), at which stage either (a) the suspension may solidify as a whole with no further motion, or (b) the interstitial melt may continue convecting within the porous, crystal framework while solidifying (Kerr & Tait 1986), and (iii) *in situ* crystal growth on the floor of the chamber.

The present study models the growth that occurs in the upper region in which spinifex-type deposits form. The model provides a mechanism by which this region may become compositionally zoned through disequilibrium effects which can cause remote solidification. However, given the cooling and solidification at the roof described here, the detailed mechanism by which the basal solid forms in a magna remains uncertain. The model presented in §3 for the growth of basal solid assumes that all the crystals fall out or grow on the floor and most closely resembles the mechanism (iii) described above. This is valid for the laboratory experiments in which crystal settling is an important process in the convecting melt, with the Stokes free-fall velocity approximately 100 times that of the typical convective velocities. However, this need not be the case in a magma.

We note, however, following the work of THS, that a qualitative comparison between figures 5 and 7 provides strong evidence of the potential importance of the

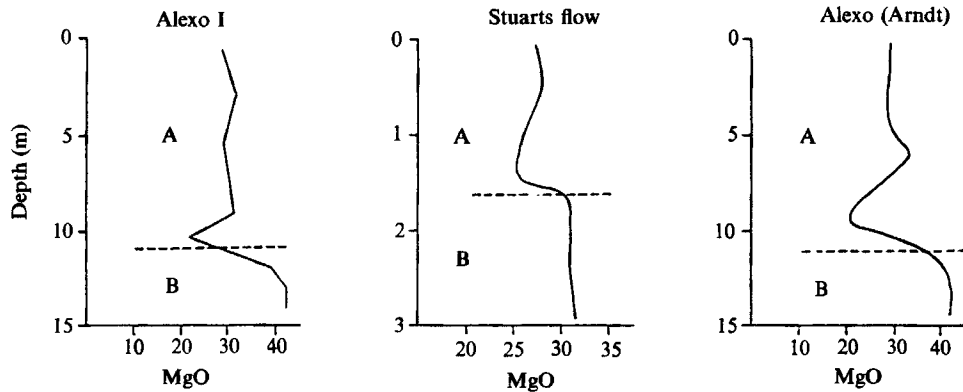


FIGURE 7. The variation with depth of the concentration of MgO in a number of solidified komatiitic lavas (taken from THS). The olivine crystals in the upper A-layer have a dendritic morphology while those of the lower B-layer are equidimensional.

present model in interpreting some features of such solidified komatiites. However, because of uncertainties in the mechanism of the basal solid growth and because of the possibility that the compositional convection generated from the basal solidification may affect the convective heat transfer in the melt (Woods & Huppert 1989), we do not make any direct quantitative predictions of the compositional profile that will result from the solidification of a magma. These effects may cause some significant changes to the rates of cooling and solidification of the melt discussed here and will form the subject of some further development of the present model (Worster, Huppert & Sparks 1990).

6. Conclusions

We have investigated both experimentally and theoretically the complete solidification of a binary alloy cooled from above at a temperature below the eutectic temperature. We have focused on the situation in which the heavy component of the melt is preferentially incorporated into the solid. In particular, we have analysed the compositional zonation and morphology of the solid formed. Following Parts 1 and 2 of this series, a model for the complete solidification which is based on local conservation of heat and composition has been developed. The composition of the final solid product decreases with depth from the initial composition of the melt towards the eutectic composition, until reaching the basal solid layer. At this point, the solid composition rapidly increases to that of the pure heavy component. This global segregation mechanism is a result of the coupling between the disequilibrium crystal growth and the melt convection. At the roof, the solid has a dendritic morphology, with composite eutectic solid bonding the dendrites, whereas nearer the floor of the tank the solid consists of a densely packed, homogeneous matrix of crystals of the heavy component of the melt.

Controlled laboratory experiments in which aqueous Na_2SO_4 of a composition beyond the eutectic was cooled from above, by a cooling plate maintained below the eutectic temperature, have confirmed the predictions of the model. The upper two-thirds of the final solid product consists of dendritic-type solid. This dendritic solid merges into the more uniform basal solid which is mainly composed of the pure solid of the heavy component of the melt and which occupies the lower third of the solid.

Following the work of THS, we have demonstrated qualitative similarities between the predictions of our model and the observed morphologies and compositional zonation of some komatiite lava deposits. The present model describes one mechanism by which such zoned deposits may be generated by disequilibrium growth kinetics and remote solidification.

We wish to thank Mark Hallworth for his technical assistance with the laboratory experiments. J. Dantzig, A. Hoadley, D. T. J. Hurle, C. Jaupart and J. S. Turner provided valuable comments and reviews. We gratefully acknowledge research fellowships from the following Cambridge Colleges: Churchill (R. C. K.), Trinity (M. G. W.) and St John's (A. W. W.), and financial support from the BP Venture Research Fund (H. E. H.). A. W. W. is also grateful for support as a Green Scholar at IGPP, Scripps Institution of Oceanography during the final stages of the research.

REFERENCES

- AMES, W. F. 1977 *Numerical Methods for Partial Differential Equations* (2nd edn). Academic.
- ARNDT, N. T. 1986 Differentiation of komatiite flows. *J. Petrol.* **27**, 279–301.
- BATCHELOR, G. K. 1974 Transport properties of two phase materials with random structure. *Ann. Rev. Fluid. Mech.* **6**, 227–255.
- CHEN, C. F. & TURNER, J. S. 1980 Crystallization in a double-diffusive system. *J. Geophys. Res.* **85**, 2573–2593.
- DENTON, R. A. & WOOD, I. R. 1979 Turbulent convection between two horizontal plates. *Intl J. Heat Mass Transfer* **22**, 1339–1346.
- DONALDSON, C. H. 1982 Spinifex textured komatiites: a review of compositions and layering. In *Komatiites* (ed. N. T. Arndt & E. G. Nisbet), Chap. 16, pp. 213–244. Allen and Unwin.
- DOREMUS, R. H. 1985 *Rates of Phase Transformations*. Academic.
- FLOOD, S. C. & HUNT, J. D. 1987 A model of a casting. *Appl. Sci. Res.* **44**, 27–42.
- GLICKSMAN, M. E. & VOORHEES, P. W. 1984 Ostwald ripening and relaxation in dendritic structures. *Metall. Trans.* **15**, 995–1001.
- HUPPERT, H. E. & SPARKS, R. S. J. 1986 Komatiites I: eruption and flow. *J. Petrol.* **26**, 694–725.
- HUPPERT, H. E. & SPARKS, R. S. J. 1988 Melting the roof of a chamber containing a hot, turbulently convecting fluid. *J. Petrol.* **29**, 559–624.
- HUPPERT, H. E., SPARKS, R. S. J., WILSON, J. R., HALLWORTH, M. A. & LEITCH, A. M. 1987 Laboratory experiments with aqueous solutions modelling processes in a magma chamber II. Cooling and crystallization along inclined planes. In *Origins of Igneous Layering* (ed. I. Parsons), pp. 539–568. Reidel.
- HUPPERT, H. E. & WORSTER, M. G. 1985 Dynamic solidification of a binary melt. *Nature* **314**, 703–707.
- KERR, R. C. & TAIT, S. 1986 Crystallisation and convection in a porous medium with application to layered igneous intrusions. *J. Geophys. Res.* **91**, 3591–3608.
- KERR, R. C. & TURNER, J. S. 1982 Layered convection and crystal layers in multi-component systems. *Nature* **298**, 731–733.
- KERR, R. C., WOODS, A. W., WORSTER, M. G. & HUPPERT, H. E. 1990a Solidification of an alloy cooled from above. Part 1. Equilibrium model. *J. Fluid Mech.* **216**, 323–342.
- KERR, R. C., WOODS, A. W., WORSTER, M. G. & HUPPERT, H. E. 1990b Solidification of an alloy cooled from above. Part 2. Non-equilibrium interfacial kinetics. *J. Fluid Mech.* **217**, 331–348.
- KURZ, W. & FISHER, D. J. 1986 *Fundamentals of Solidification*. Trans Tech Publications.
- MARTIN, D. & NOKES, R. I. 1988 Crystal settling in a vigorously convecting magma chamber. *Nature* **332**, 534–536.
- MARTIN, D. & NOKES, R. I. 1989 A fluid-dynamical study of crystal settling in convecting magma chambers. *J. Petrol.* **30** 1471–1500.

- TURNER, J. S., HUPPERT, H. E. & SPARKS, R. S. J. 1986 Komatiites II. Experimental and theoretical investigations of post-emplacement cooling and crystallization. *J. Petrol.* **27**, 397-437 (herein referred to as THS).
- WEAST, R. C. (ed.) 1971 *CRC Handbook of Chemistry and Physics*. The Chemical Rubber Co.
- WOODS, A. W. & HUPPERT, H. E. 1989 The growth of compositionally stratified solid by cooling a binary alloy from below. *J. Fluid Mech.* **199**, 29-55.
- WORSTER, M. G. 1986 Solidification of an alloy from a cooled boundary. *J. Fluid Mech.* **167**, 481-501.
- WORSTER, M. G., HUPPERT, H. E. & SPARKS, R. S. J. 1990 Convection and crystallization in magma cooled from above. *Earth Planet. Sci. Lett.* (in press).